Korean J Physiol Pharmacol 2020;24(1):111-119
https://doi.org/10.4196/kjpp.2020.24.1.111

KJPP

Original Article

Decreased inward rectifier and voltage-gated K^+ currents of the right septal coronary artery smooth muscle cells in pulmonary arterial hypertensive rats

Sung Eun Kim[1,2,#], Ming Zhe Yin[1,2,#], Hae Jin Kim[1,2], Rany Vorn[3], Hae Young Yoo[3,*], and Sung Joon Kim[1,2,4,*]

Departments of [1]Physiology and [2]Biomedical Sciences, Seoul National University College of Medicine, Seoul 03080, [3]Department of Nursing, Chung-Ang University, Seoul 06974, [4]Ischemic/Hypoxic Disease Institute, Seoul National University College of Medicine, Seoul 03080, Korea

ARTICLE INFO

Received October 10, 2019
Revised November 28, 2019
Accepted November 28, 2019

***Correspondence**
Sung Joon Kim
E-mail: physiolksj@gmail.com
Hae Young Yoo
E-mail: hyoo@cau.ac.kr

Key Words
Coronary artery
Inward rectifier K^+ channel
Pulmonary arterial hypertension
Potassium channel
Smooth muscle

[#]These authors contributed equally to this work.

ABSTRACT In vascular smooth muscle, K^+ channels, such as voltage-gated K^+ channels (Kv), inward-rectifier K^+ channels (Kir), and big-conductance Ca^{2+}-activated K^+ channels (BK_{Ca}), establish a hyperpolarized membrane potential and counterbalance the depolarizing vasoactive stimuli. Additionally, Kir mediates endothelium-dependent hyperpolarization and the active hyperemia response in various vessels, including the coronary artery. Pulmonary arterial hypertension (PAH) induces right ventricular hypertrophy (RVH), thereby elevating the risk of ischemia and right heart failure. Here, using the whole-cell patch-clamp technique, we compared Kv and Kir current densities (I_{Kv} and I_{Kir}) in the left (LCSMCs), right (RCSMCs), and septal branches of coronary smooth muscle cells (SCSMCs) from control and monocrotaline (MCT)-induced PAH rats exhibiting RVH. In control rats, (1) I_{Kv} was larger in RCSMCs than that in SCSMCs and LCSMCs, (2) I_{Kv} inactivation occurred at more negative voltages in SCSMCs than those in RCSMCs and LCSMCs, (3) I_{Kir} was smaller in SCSMCs than that in RCSMCs and LCSMCs, and (4) I_{BKCa} did not differ between branches. Moreover, in PAH rats, I_{Kir} and I_{Kv} decreased in SCSMCs, but not in RCSMCs or LCSMCs, and I_{BKCa} did not change in any of the branches. These results demonstrated that SCSMC-specific decreases in I_{Kv} and I_{Kir} occur in an MCT-induced PAH model, thereby offering insights into the potential pathophysiological implications of coronary blood flow regulation in right heart disease. Furthermore, the relatively smaller I_{Kir} in SCSMCs suggested a less effective vasodilatory response in the septal region to the moderate increase in extracellular K^+ concentration under increased activity of the myocardium.

INTRODUCTION

Ion channels in arterial smooth muscle regulate the membrane potential, Ca^{2+} permeability, and vascular tone, and maintain homeostasis [1]. There are several types of K^+ channels in arterial smooth muscle cells (SMCs). Voltage-gated K^+ channels (Kv) are activated by membrane depolarization to induce membrane repolarization and prevent excessive Ca^{2+} influx through L-type Ca^{2+} channels [2,3]. Inward rectifier K^+ channels (Kir) contribute to the establishment of a hyperpolarized membrane potential and mediate endothelium-dependent hyperpolarization and the active hyperemia response in various vessels, including the coronary artery (CA) [4,5]. Big-conductance Ca^{2+}-activated K^+ channels (BK_{Ca}) are abundantly expressed in SMCs and are activated in concert by membrane depolarization and increased concentrations of cytosolic Ca^{2+} ($[Ca^{2+}]_c$) to provide a negative feedback regulatory component in the arterial smooth muscle [6].

Compared with the current knowledge of K^+ channels in arte-

Author contributions: S.J.K. and H.Y.Y. supervised and coordinated this study. S.E.K., M.Z.Y., and H.J.K. performed the experiments. S.E.K., M.Z.Y., H.J.K., S.J.K., and R.V. analyzed and interpreted the data. S.E.K., H.Y.Y., S.J.K., and R.V. prepared the manuscript.

rial smooth muscle, our understanding of K^+ channels in the CA, especially regarding the branches perfusing different areas of the heart, is limited. As major trunks of the CA originating from the initial segment of the aorta, the left coronary arteries (LCAs)—which are divided into left anterior descending (LAD) and left circumflex coronary (LCX) arteries—are located between the pulmonary artery and the left atrial appendage and flow to the left ventricular (LV) walls and partly, to the septum. The right coronary arteries (RCAs) are located on the right side of the heart and perfuse the right ventricular (RV) walls and the septal area. Septal coronary arteries (SCAs) originate from both LCAs and RCAs [7].

Coronary circulation provides oxygen and nutrients to the cardiomyocytes, and its impairment causes major cardiac diseases, such as ischemic heart disease [8]. Several studies have demonstrated that impaired coronary circulation is also related to right heart diseases associated with pulmonary arterial hypertension (PAH) and RV hypertrophy (RVH) [9-11]. PAH is a lethal vascular disease characterized by high pulmonary arterial pressure (> 25 mmHg) and progressive remodeling of the pulmonary vasculature [12]. The increased afterload to the RV causes RVH in PAH patients and can inhibit adequate CA blood flow to the RV, thereby increasing the risk of ischemia and RV failure. Various animal models have been used to identify the underlying mechanisms associated with PAH [13]. Among these, the monocrotaline (MCT)-induced PAH model involving single injection of MCT in rats has been widely used [14], with numerous studies reporting the functional roles of pulmonary arterial smooth muscle and endothelial dysfunction in MCT-induced PAH (MCT-PAH) [15-17].

Interestingly, a recent study reported CA remodeling, including thickening of the vascular wall, in patients with PAH as well as in MCT-PAH models [18]. Given the plausible elevated risk of ischemic damage to the RV, branch-specific changes in K^+ channel currents in CA smooth muscle would be an intriguing research topic; however, most studies on arterial smooth muscle in PAH have focused on pulmonary arteries [15-17].

Regarding the comparison of K^+ channel activities between RCAs and LCAs, a previous study demonstrated higher levels of Kv1.2-type current showing slow inactivation in RCA SMCs (RCSMCs) than that in LCA SMCs (LCSMCs) of healthy Wistar rats [19]. In contrast, another study reported that non-inactivating Kv7-type current was increased in LCSMCs than that in RCSMCs of healthy rats [19,20]. Moreover, a previous study using a PAH disease model of chronic hypoxia showed that Kv1.2- and Kv1.5-type currents were decreased in RCAs than those in LCAs [21].

In the present study, we elucidated the changes in K^+ channel currents in CA myocytes isolated from MCT-PAH model rats, with special focus on branch-specific comparisons. We initially compared the densities of three major types of K^+ channel current (I_{Kv}, I_{Kir}, I_{BKCa}) between LCSMCs, RCSMCs, and SMCs from the septal branch from the main trunk of the right CA (SCSMCs).

METHODS

Animals

All experimental procedures were performed with the approval of the Institutional Animal Care and Use Committee (IACUC) of Seoul National University (IACUC approval no: 170626-3-1). Male Sprague–Dawley rats (230–280 g) were used for all experiments. MCT-induced PAH was developed by a single intraperitoneal (i.p.) injection of MCT (60 mg/kg; Sigma-Aldrich, St. Louis, MO, USA) into 7-to-8-week-old rats; control rats were injected with an equal amount of saline. After 3 weeks, MCT-injected rats (hereafter referred to as MCT-PAH rats) were euthanized. All rats were anaesthetized by i.p. injection of a ketamine and xylazine mixture (ketamine 90 mg/kg and xylazine 10 mg/kg).

RVH histology

For histological analysis, hearts were fixed in 4% paraformaldehyde overnight, and paraffin-embedded tissue sections were cut (5 μm thickness) and stained with hematoxylin and eosin (H&E). Digital images of stained tissues were obtained at a magnification of 200× using an Olympus BX51 (Olympus, Tokyo, Japan) and Photoshop 7.0 software (Adobe, San Jose, CA, USA) (Fig. 1A). The RVH index was calculated as a ratio of the RV weight versus the composite weight of the LV and septum (S) as follows: RVH index = RV/(LV+S) (Fig. 1B).

Preparation of vessels and single myocyte isolation

CAs were dissected under a surgical microscope (SMZ645; Nikon, Tokyo, Japan). The LCAs used in this study included first and second branches of the LAD and LCX arteries located on the surface of the heart. In addition, RCA branches were dissected from the surface of the RV, and SCAs were dissected from the surface of the internal cavity of the RV (Fig. 1E). After dissection of the arteries, vessels were incubated in the first digestion medium (nominal Ca^{2+}-free normal Tyrode (NT) solution containing 1 mg/ml papain; Sigma-Aldrich) for 17 min, followed by incubation in the second digestion medium (nominal Ca^{2+}-free NT solution containing 3 mg/ml collagenase; Wako Pure Chemical, Osaka, Japan) for 13 min. Both digestion media contained bovine serum albumin (1 mg/ml; Calbiochem, Billerica, MA, USA) and dithiothreitol (1 mg/ml; Sigma-Aldrich).

Electrophysiology

Whole-cell patch-clamp experiments were performed using a patch-clamp amplifier (Axopatch-200A; Axon Instruments, Foster City, CA, USA). We used pCLAMP software (v.10.4) and Digidata-1440A (Axon Instruments) to acquire data and to apply the command pulse. Current recordings were made at room

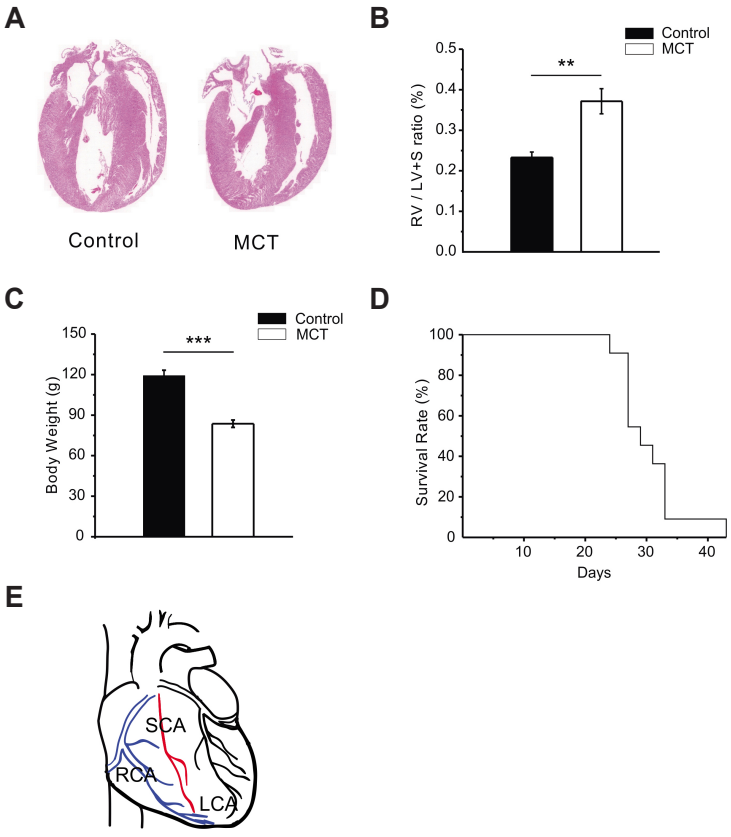

Fig. 1. Indices of monocrotaline (MCT)-injected rats (MCT-PAH rats) and coronary artery (CA) dissection areas. At 3 weeks post treatment, control and MCT rats showed variations in key indicators. (A, B) Representative images of histological sections of the whole heart from control and MCT rats. The right ventricular (RV) wall in MCT rats shows thickening compared with that in control rats. RV hypertrophy (RV/LV+S) is shown as a bar graph. (C) Body weight (g) was smaller in MCT (n = 37) than that in control (n = 36) rats. (D) Survival rates of MCT rats (n = 12); after 30 days, 90% of the rats were dead. (E) Left CAs (LCAs) (*black*), including the left circumflex arteries and left anterior descending arteries, right CAs (RCAs) (*blue*), and septal CAs (SCAs) (*red*). PAH, pulmonary arterial hypertension; LV, left ventricular; S, septum. Data represent the mean ± standard error of the mean. **p < 0.01; ***p < 0.001; unpaired Student's t-test.

temperature (23°C–25°C), using glass microelectrodes with a resistance of approximately 2.5–3.0 MΩ. Membrane capacitance of each cell was measured and was used to normalize the current amplitude (i.e., current density [pA/pF]).

Experimental solutions and chemicals

The pipette solution for recording I_{Kv} and I_{Kir} contained 120 mM K-aspartate, 20 mM KCl, 10 mM HEPES, 1 mM $MgCl_2$, 3 mM MgATP, and 5 mM EGTA (adjusted to pH 7.2 with KOH). The NT external solution comprised 140 mM NaCl, 5.4 mM KCl, 10 mM HEPES, 10 mM glucose, 1 mM $MgCl_2$, and 1.8 mM $CaCl_2$ (adjusted to pH 7.4 with NaOH). For I_{Kir}, symmetric high-K^+ 140 mM KCl bath solution (KCl solution) was used (140 mM KCl, 10 mM HEPES, 10 mM glucose, 1.8 mM $CaCl_2$, and 1 mM $MgCl_2$ [adjusted to pH 7.4 with KOH]). After confirming the steady-state current under symmetrical high-K^+ conditions, 100 μM $BaCl_2$ was administered to block the inward K^+ current component in order to selectively calculate the density of I_{Kir}. For the I_{BKCa} channel recording, the pipette solution contained 120 mM K aspartate, 20 mM KCl, 10 mM HEPES, 3 mM MgATP, 10 mM EGTA, 1 mM $MgCl_2$, and 8.6 mM $CaCl_2$ (pH 7.2), with the free Ca^{2+} concentration fixed at 1 μM.

Statistical analysis

Data are reported as original recordings and bar graphs of the mean ± standard error of the mean. Means were compared using unpaired Student's t-tests. Statistical significance was defined as $p < 0.05$.

RESULTS

Compared with control rats, MCT rats showed a thickened RV wall (Fig. 1A), as well as a significantly increased RVH index [RV/(LV+S)] (control rats: 0.2 ± 0.01, n = 7; MCT rats: 0.4 ± 0.03, n = 6; $p < 0.01$) (Fig. 1B). At 3 weeks after MCT injection, the body weights (g) of MCT-injected rats were lower than those of age-matched controls (control rats: 119.2 ± 4.02 g, n = 36; MCT rats:

83.7 ± 2.71, n = 37; p < 0.001) (Fig. 1C). At 30 days after injection, < 10% of MCT rats survived (Fig. 1D).

Smaller I_{Kv} in SCSMCs

In the whole-cell patch-clamp configuration study, I_{Kv} was activated by membrane depolarization from a −80 mV holding voltage with 5 mM EGTA-containing KCl pipette solution. Step-like depolarization ranging from −50 mV to 40 mV induced outward currents showing slow inactivation during a 2.5-s pulse period (Fig. 2). Peak outward currents normalized to the membrane capacitance (i.e., pA/pF) were determined in order to compare the level of Kv activity. Although a buffer with high-concentration of Ca^{2+} (5 mM EGTA) was included in the pipette solution, we also examined the effect of paxilline, a highly selective and potent blocker of BK_{Ca}, in order to exclude I_{BKCa} activation by strong depolarization. Paxilline application did not affect the amplitudes of the peak outward currents, indicating that the recordings obtained using the 5 mM EGTA pipette solution were not contaminated by I_{BKCa} (Fig. 2G).

The I_{Kv} densities were similar in control LCSMCs (12.7 ± 1.45 pA/pF at +40 mV, n = 27) and control SCSMCs (12.3 ± 1.08 pA/pF at +40 mV, n = 15), but higher in control RCSMCs (19.8 ± 2.44 pA/pF at +40 mV, n = 17) (Fig. 2H). Comparison of control and MCT-PAH rats revealed that the I_{Kv} densities in LCSMCs and RCSMCs did not differ (Fig. 2A, B, E, F), whereas they were lower in SCSMCs from MCT-PAH rats than in those from control rats (12.3 ± 1.08 pA/pF *vs.* 8.8 ± 0.95 pA/pF at +40 mV, n = 15) (Fig. 2C, D). Additionally, the I/V curves showed that the current densities in MCT-PAH SCSMCs were significantly decreased at 20 mV, 30 mV, and 40 mV (p < 0.05) (Fig. 2D), and that the current densities in control RCSMCs were significantly greater than those

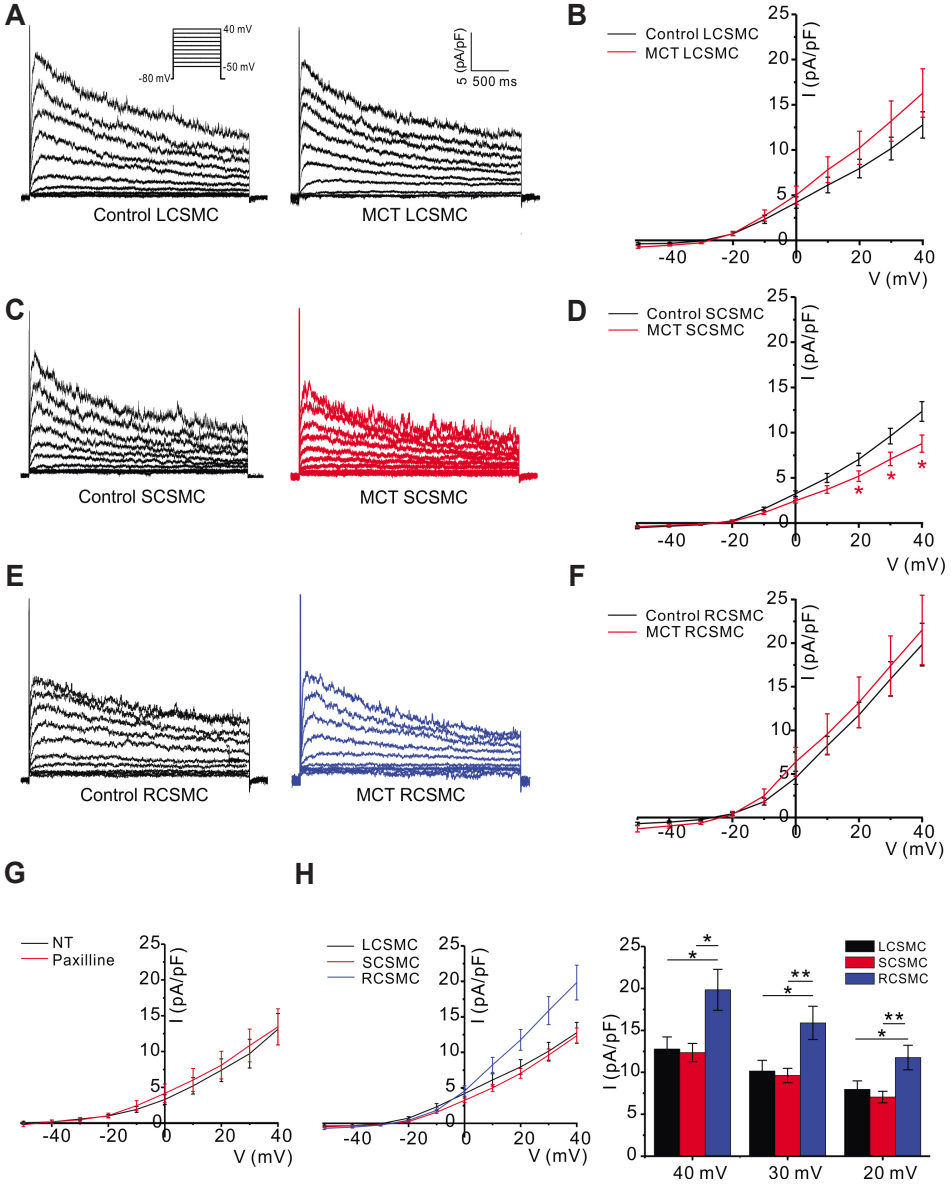

Fig. 2. Comparison of voltage-gated K^+ channel currents (I_{Kv}) in control and monocrotaline (MCT)-induced pulmonary arterial hypertension (PAH) coronary artery (CA) smooth muscle cells (SMCs). I_{Kv} in three types of CA SMCs. For whole-cell patch-clamp experiments, depolarizing step pulses from −50 to 40 mV were applied at 5 s intervals (holding voltage: −80 mV; interval voltage: 10 mV). (A, B) Representative traces of LCA SMCs (LCSMCs) in control and MCT rats. Averaged I/V curves for LCSMCs from control (n = 27) and MCT (n = 14) rats. I_{Kv} was slightly, but not significantly increased in MCT-PAH rats. (C, D) Representative traces of SMCs from the septal branch from the main trunk of the right CA (SCSMCs) in control and MCT rats. Averaged I/V curves for SCSMCs from control (n = 15) and MCT (n = 15) rats revealed decreased I_{Kv} in MCT rats relative to that in controls. (E, F) Representative traces of RCA SMCs (RCSMCs) in control and MCT-PAH rats. Averaged I/V curves for RCSMCs from control (n = 17) and MCT (n = 13) rats showing similar current densities. (G) Addition of paxilline (1 μM; a BK_{Ca} channel inhibitor) to normal Tyrode (NT) had no effect on I_{Kv} current densities. (H) According to averaged I/V curves, current densities in control RCSMCs were significantly greater than those in control LCSMCs and SCSMCs. Data represent the mean ± standard error of the mean. *p < 0.05; **p < 0.01; unpaired Student's t-test.

https://doi.org/10.4196/kjpp.2020.24.1.111

in control LCSMCs ($p < 0.05$) and SCSMCs ($p < 0.01$).

Voltage-dependent inactivation of I_{Kv}

The raw traces of I_{Kv} revealed slow inactivation during the depolarizing pulses (Fig. 2A, C, E). Because the resting membrane potential of vascular smooth muscle usually exists at relatively depolarized levels (i.e., −40 to −60 mV), the steady-state level of partially inactivated I_{Kv} would represent the effective outward current. Therefore, we analyzed the voltage dependence of inactivation using a double-pulse protocol. Different levels of long pre-pulses (10 s) were applied, immediately followed by a +40-mV test pulse for 30 ms (Fig. 3A). The normalized amplitudes at the test pulse were plotted against the various depolarizing pre-pulses, which reflected the voltage-dependent inactivation. The voltage dependences illustrated by the inactivation curves were obtained by fitting the data to the Boltzmann equation. The half-inactivation voltage ($V_{1/2}$) of control SCSMCs (−40.1 ± 1.58 mV) was more negative than that of control LCSMCs (−31.0 ± 0.74 mV) and RCSMCs (−29.3 ± 1.51 mV) (Fig. 3B). Interestingly, the $V_{1/2}$ of MCT-PAH SCSMCs was shifted slightly toward the right (−35.0 ± 0.83 mV), and $V_{1/2}$ was not significantly different between MCT-PAH LCSMCs (−30.6 ± 0.86 mV) and MCT-PAH RCSMCs (−30.3 ± 1.62 mV) (Fig. 3C).

Next, we analyzed the voltage-dependent activation property using the Boltzmann equation after plotting the normalized conductance (G/G_{max}) of outward currents against the test voltages. The voltage-dependent activation tended to be similar between control and MCT-PAH rats. The $V_{1/2}$ of both control LCSMCs (−6.1 ± 1.61 mV) and MCT LCSMCs (−5.5 ± 1.33 mV) was shifted toward the left, whereas that of SMCs from other arteries was not (Fig. 3D, E). Control RCSMCs (5.8 ± 0.79 mV) and control

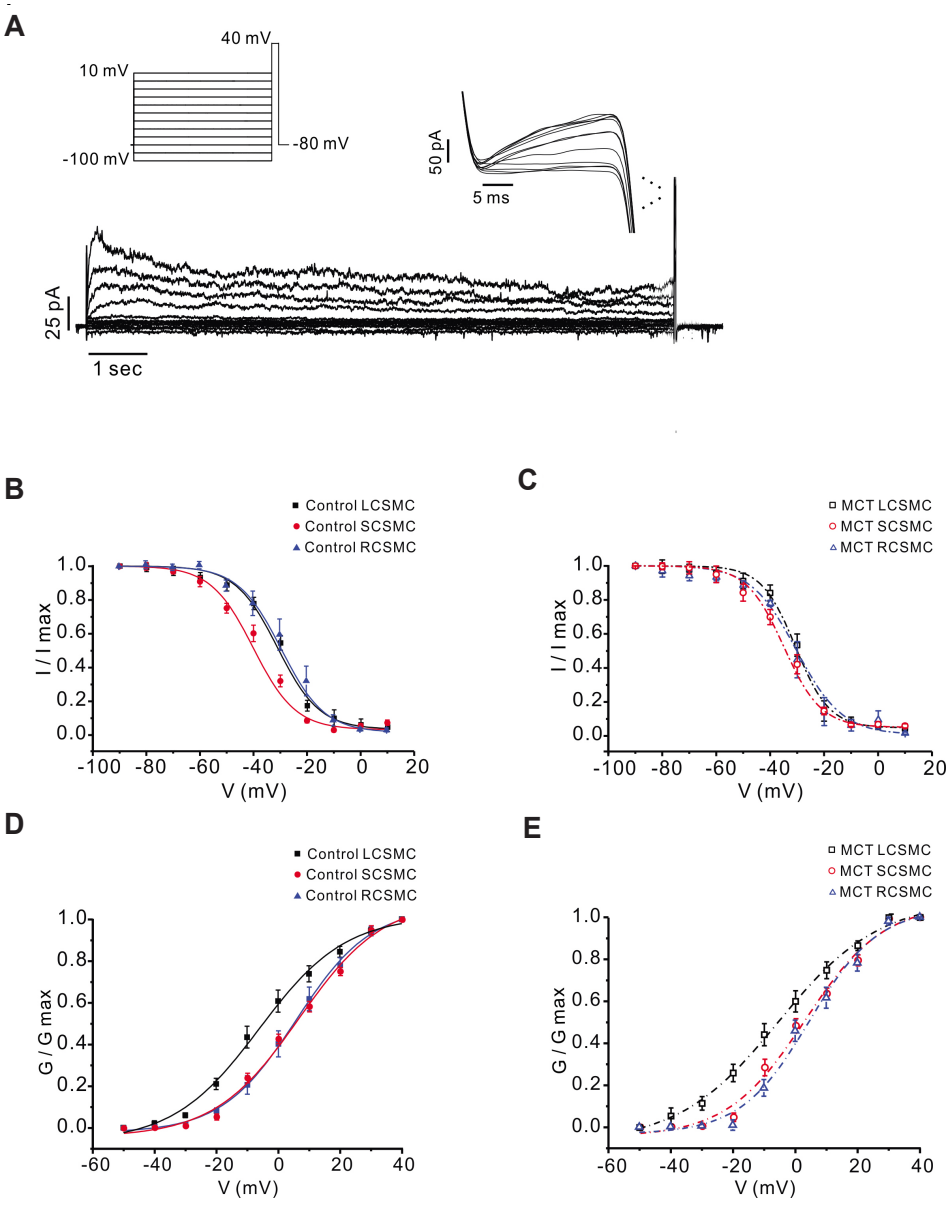

Fig. 3. Inactivation kinetics of I_{Kv} in coronary artery (CA) smooth muscle cells (SMCs). Inactivation occurred at a more negative voltage in SCSMCs than that in LCSMCs and RCSMCs. (A) Representative K^+ current traces for the analysis of voltage-dependent I_{Kv} inactivation. Two step pulses were required for the generation of the inactivation curves. Pre-sustained pulses (−100 to +10 mV, with 10-mV intervals) were applied for 10 s, immediately followed by +40 mV test pulses for 30 ms. (B) Voltage-dependent inactivation curves of I_{Kv} measured in control LCSMCs (*black*), SCSMCs (*red*), and RCSMCs (*blue*). Curves were fitted using the Boltzmann equation. Unlike for LCSMCs (−31.0 ± 0.74 mV; *black*) and RCSMCs (−29.3 ± 1.52 mV; *blue*), the curve for SCSMCs (−40.1 ± 1.59 mV; *red*), showed a shift to the left. (C) Similarly, voltage-dependent inactivation curves of I_{Kv} for monocrotaline (MCT)-SCSMCs (−35.0 ± 0.83 mV; *red*) were shifted to the left, in contrast to those for MCT-RCSMCs (−30.3 ± 1.62 mV) and MCT-LCSMCs (−30.6 ± 0.86 mV). (D) Voltage-dependent activation curves of I_{Kv} were generated for control LCSMCs (−6.1 ± 1.61 mV; *black*), SCSMCs (6.6 ± 2.12 mV; *red*), and RCSMCs (5.8 ± 0.79 mV; *blue*), and were fitted using the Boltzmann equation to fit G/G_{max}. Control LCSMCs had a more negative voltage than SMCs from other arteries. (E) Voltage-dependent activation curves of I_{Kv} for MCT-LCSMCs (−5.5 ± 1.33 mV) were shifted to the left in contrast to those for MCT-SCSMCs (3.1 ± 2.27 mV; *red*) and MCT-RCSMCs (4.6 ± 2.01 mV).

SCSMCs (6.6 ± 2.12 mV) had similar current densities, as did the MCT RCSMCs (4.6 ± 2.01 mV) and MCT SCSMCs (3.1 ± 2.27 mV).

I_{Kir} in CA myocytes from control and PAH-MCT rats

For selective recording of I_{Kir}, the bath solution was changed from an NT to a KCl solution, and the membrane voltage was maintained at 0 mV. We applied a ramp-like hyperpolarizing pulse from 30 to –140 mV, and the brief I/V curve obtained by the ramp pulse showed an inwardly rectifying current, which was abolished by applying 100 μM Ba^{2+}, a Kir blocker (Fig. 4A). The Ba^{2+}-sensitive current reflecting I_{Kir} was obtained by digital subtraction and compared between the three branches (Fig. 4B). The I_{Kir} densities at –140 mV were significantly smaller in control SCSMCs (–11.9 ± 2.46 pA/pF, n = 13, $p < 0.05$) than that in control LCSMCs (–18.0 ± 1.76 pA/pF, n = 17) and control RCSMCs (–17.1 ± 2.47 pA/pF, n = 16) (Fig. 4C). Interestingly, the I_{Kir} densities of MCT-PAH SCSMCs (–5.0 ± 0.59 pA/pF, n = 21) were even smaller than those of control SCSMCs (–11.9 ± 2.46 pA/pF, n = 13; $p < 0.001$) (Fig. 4D). In contrast, the I_{Kir} densities of RCSMCs and LCSMCs did not differ between the control and MCT-PAH (Fig. 4D).

I_{BK} of CA myocytes from control and MCT-PAH

To record I_{BKCa}, we used a KCl pipette solution with 1 μM of free Ca^{2+} buffered with 10 mM EGTA. Because BK_{Ca} is not inactivated at the depolarized membrane potential, we applied a ramp-like hyperpolarizing pulse from 50 mV to –100 mV at the depolarized holding voltage (–10 mV) in order to induce I_{Kv} inactivation. The outwardly rectifying current was completely abolished by addition of 1 μM of paxilline, indicating selective recording of I_{BKCa} in CA myocytes (Fig. 5A). I_{BKCa} density did not differ between myocytes of the three CA branches in controls (Fig. 5B), and no significant difference in I_{BKCa} was observed between control and MCT-PAH CA myocytes (Fig. 5C–E).

DISCUSSION

We investigated the functional remodeling of the three types of K^+ channel currents in SMCs obtained from the three branches of the CA in MCT-PAH and control rats. Although we initially hypothesized that the measured parameters might differ to a greater degree in RCSMCs than that in LCSMCs and SCSMCs, we mainly observed intriguing differences in SCSMCs.

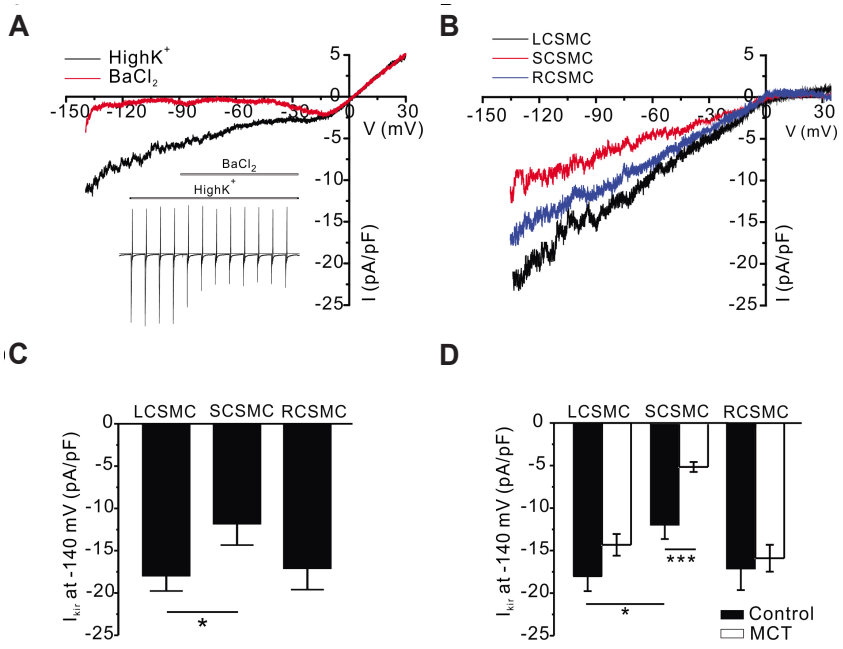

Fig. 4. I_{Kir} in coronary artery (CA) smooth muscle cells (SMCs). I_{Kir} in control and monocrotaline (MCT)-pulmonary arterial hypertension (PAH) SCSMCs decreased significantly. (A) Representative traces of I_{Kir} in control rats were elicited by applying depolarizing ramp-like pulses from –140 mV to 30 mV, following perfusion of 140 mM symmetrical high-K^+ solution containing 100 μM $BaCl_2$. (B) Averaged I/V curves of Ba^{2+}-sensitive current (high-K^+ current with 100 μM Ba^{2+}) in symmetrical K^+ solution. (C) Bar graphs showing the Ba^{2+}-sensitive current in control LCSMCs (n = 17), SCSMCs (n = 13), and RCSMCs (n = 16) measured at –140 mV. I_{Kir} in SCSMCs was smaller than that in LCSMCs and RCSMCs, with a significant difference observed between I_{Kir} in SCSMCs and LCSMCs. (D) Summary of the Ba^{2+}-sensitive current in SMCs from control and MCT rats: MCT-PAH LCSMCs (n = 19), MCT-PAH SCSMCs (n = 21), MCT-PAH RCSMCs (n = 18). The Ba^{2+}-sensitive current in MCT-PAH SCSMCs was significantly lower than that in MCT-PAH LCSMCs and MCT-PAH RCSMCs. Data represent the mean ± standard error of the mean. *$p < 0.05$; ***$p < 0.001$; unpaired Student's t-test.

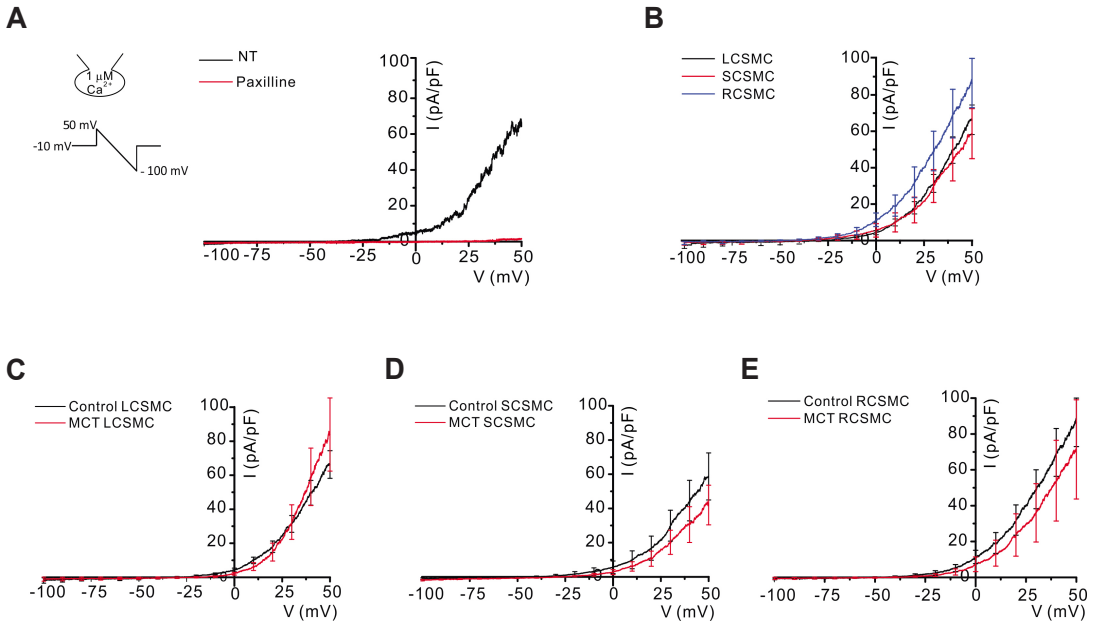

Fig. 5. BK_{Ca} and I_{BKCa} in coronary artery (CA) smooth muscle cells (SMCs). We observed no differences in I_{BKCa} between CA SMCs. For whole-cell patch-clamp experiments, we applied reverse depolarizing ramp-like pulses from 50 mV to −100 mV (holding at −10 mV). Paxilline (1 μM) administration blocked a large component of the outward currents. (A) Representative traces of I_{BKCa} in control rats. Currents were recorded in normal Tyrode (NT) solution (*black*) containing 1 μM paxilline (*red*). (B) Averaged I/V curves for control LCSMCs (n = 10, *black*), SCSMCs (n = 8, *red*), and RCSMCs (n = 8, *blue*), show no significant differences. (C–E) Comparison of I_{BKCa} in SMCs from control and MCT rats reveal no significant differences between control (n = 10) and MCT LCSMCs (n = 8), control (n = 8) and MCT SCSMCs (n = 7), and control (n = 8) and MCT RCSMCs (n = 8).

Different levels of I_{Kv} among CA branches from control rats and changes associated with PAH

Electrophysiological analyses of control rats demonstrated branch-specific differences in K^+ currents, including higher I_{Kv} in RCSMCs and lower I_{Kir} in SCSMCs (Figs. 2H and 4C). Similarly, a previous comparative study of I_{Kv} between RCSMCs and LCSMCs reported a higher peak amplitude in RCSMCs than that in LCSMCs [19], although SCSMCs were not investigated in this study. Another study revealed that the Kv7-type current of I_{Kv} was larger in LCSMCs than that in RCSMCs, but total Kv currents were not compared between LCA and RCA [20], which makes it difficult to compare these findings with our results. We attempted to measure and compare Kv7-sensitive currents using linopirdine, a Kv7 inhibitor; however, linopiridine-sensitive currents were too small to distinguish the differences between LCA and RCA (data not shown). A previous study that compared Kv7 currents in the cerebral artery and CA reported that responses of Kv7 currents in CA SMCs to linopirdine were blunted when compared to those in cerebral artery SMCs, and Kv7 component in total K^+ conductance was relatively small [22]. Our results partially agree with those reported by Gautier *et al*. [19], in that the peak amplitude of I_{Kv} in control RCSMCs was larger than that in the other branches (Fig. 2H). However, because the difference in I_{Kv} was not significant at the physiological range of negative membrane voltages, the physiological implications of the higher I_{Kv} density *in vivo* remain to be explored. Rather than the peak amplitude, the difference in steady-state inactivation at the negative membrane voltage requires further attention. The I_{Kv} in SCSMCs showed more sensitive voltage-dependent inactivation (i.e., a more negative $V_{1/2}$), suggesting a relatively smaller steady-state conductance in SCSMCs than that in the other branches. Furthermore, the I_{Kir} density in SCSMCs was smaller than that in RCSMCs and LCSMCs.

Previous comparisons of I_{Kv} between RCAs and LCAs were conducted in rat models of hyperglycemia and chronic hypoxia [20,21]. Hyperglycemic rats showed a decrease in Kv7 current density, which was more prominent in LCSMCs than in RCSMCs [20], whereas in a chronic hypoxia state that led to PAH, Kv current densities were decreased in RCSMCs, but increased in LCSMCs [21]. Notably, these studies did not examine the I_{Kv} in SCSMCs. In the present study, using CA myocytes from MCT-PAH rats, we observed no significant changes in the I_{Kv} in LCSMCs and RCSMCs, whereas that in SCSMCs consistently decreased. However, we noted a slight shift to the rightward direction for the inactivation curve for SCSMCs (Fig. 3B, C), which might have partly compensated for the decrease in the peak current density of I_{Kv}. The discrepant results might be explained by the different types of disease models.

Different levels of I_{Kir} among CA branches from control rats and changes associated with PAH

Kir in arterial myocytes are generally more abundant in ves-

sels with a smaller diameter, and thereby contribute to the resting membrane potential and basal tone of the arteries [23]. Although the functional expression of Kir in CA myocytes has been reported in pigs [23], rabbits [24], and rats [25], differences in I_{Kir} among the major branches of CAs have not been studied. Furthermore, to the best of our knowledge, decreased I_{Kir} in CA myocytes from PAH animal models has never been investigated.

Kir activity is facilitated by extracellular K^+ activity ($[K^+]e$) and represents the underlying mechanism of membrane hyperpolarization under moderate increases in $[K^+]e$. Moreover, the hyperpolarization and subsequent relaxation of Kir-expressing arteries underlie $[K^+]e$-induced vasorelaxation, which is critical for matching the regional blood flow to electrically excitable tissues, such as myocardium. In this respect, the lower I_{Kir} observed in SCSMCs and its attenuation associated with MCT-PAH might imply a putatively higher risk of impaired blood supply in the septal region of the RV cavity. Regretfully, we were unable to experimentally explain the different levels of I_{Kir} in SCSMCs.

Implications of lower K^+ conductance in SCSMCs

As noted, in addition to the smaller I_{Kir}, the voltage-dependent inactivation of Kv appeared to be more sensitive in SCSMCs than that in the other branches in control rats. However, the I_{BKCa} density did not differ between the branches, and no significant changes were observed in MCT-PAH rats (Fig. 5). The SCA used in this study was a branch of the RCA trunk and was dissected from the septal myocardium of the RV. While the RCA and LCA branches were dissected from the surface of the rat heart, the SCA in the relatively deep region might be exposed to higher mechanical stress in the RVH myocardium. Although we currently have no experimental evidence of this activity, it is possible that the putatively different levels of mechanical stress might be associated with the different electrophysiological properties of SCSMCs.

A previous study reported a decrease in right coronary blood flow in PAH patients, and suggested that such a decrease in blood flow could possibly contribute to RVH [10]. Coronary blood flow shows a phasic pattern throughout the cardiac cycle. During systole, the left coronary blood flow is impeded due to squeezing force, but the RCA is relatively much less affected [7]. However, in RVH, the RCA flow becomes biphasic, with reduced systolic and increased diastolic flow. Due to the increase in RV pressure, systolic coronary flow is impeded in PAH patients. The reduced blood flow from the RCA might lead to RV ischemia, which contributes to RV failure. Due to the enlarged RV, the impairment of systolic coronary blood flow in the SCAs might be induced by compression pressure from the LV and RV in PAH with RVH. Accordingly, structural remodeling of the CA wall in RV has been observed in PAH patients and rat models [18]. Although we currently do not have direct evidence, given the anatomical location of the SCAs used in the present study, we suggest that the functional downregulation of I_{Kir} in SCSMCs might also occur in the CAs of patients with PAH. The lower Kir and Kv conductance of SCSMCs observed in the present study might be associated with reduced coronary blood flow and CA remodeling in PAH with RVH. Further studies are needed to elucidate the physiological role of K^+ currents on blood flow and histological changes in septal CAs.

In summary, this was the first study to comprehensively compare K^+ channels in vascular SMCs of CAs from three different branches. The results revealed not only the differential densities of K^+ currents, but also branch-specific changes in current amplitudes in PAH-induced RVH. The attenuation of I_{Kir} in SCSMCs from a rat MCT-PAH model offered insights into the pathophysiology of the increased risk of RV failure in PAH. Since structural remodeling of the CA wall has been reported in PAH [18], our findings suggest a possible functional remodeling of the CA in PAH-induced RVH.

ACKNOWLEDGEMENTS

This work was supported by a National Research Foundation of Korea (NRF) funded by the Ministry of Science and ICT of the Republic of Korea (grant nos. NRF-2018R1A5A2025964 and NRF-2018R1D1A1B07048998 to S.J. Kim, NRF-2019R1-F1A1062965 to H.Y. Yoo). In addition, this work was supported by the Education and Research Encouragement Fund of Seoul National University Hospital (2019).

CONFLICTS OF INTEREST

The authors declare no conflicts of interest.

REFERENCES

1. Werner ME, Ledoux J. K^+ channels in biological processes: vascular K^+ channels in the regulation of blood pressure. *J Receptor Ligand Channel Res.* 2014;7:51-60.
2. Nelson MT, Quayle JM. Physiological roles and properties of potassium channels in arterial smooth muscle. *Am J Physiol.* 1995;268(4 Pt 1):C799-C822.
3. An JR, Li H, Seo MS, Park WS. Inhibition of voltage-dependent K^+ current in rabbit coronary arterial smooth muscle cells by the class Ic antiarrhythmic drug propafenone. *Korean J Physiol Pharmacol.* 2018;22:597-605.
4. Knot HJ, Zimmermann PA, Nelson MT. Extracellular K^+-induced hyperpolarizations and dilatations of rat coronary and cerebral arteries involve inward rectifier K^+ channels. *J Physiol.* 1996;492 (Pt 2):419-430.
5. Longden TA, Nelson MT. Vascular inward rectifier K^+ channels as external K^+ sensors in the control of cerebral blood flow. *Microcirculation.* 2015;22:183-196.
6. Dopico AM, Bukiya AN, Jaggar JH. Calcium- and voltage-gated BK

channels in vascular smooth muscle. *Pflugers Arch.* 2018;470:1271-1289.
7. Gregg DE. The coronary circulation. *Physiol Rev.* 1946;26:28-46.
8. Goodwill AG, Dick GM, Kiel AM, Tune JD. Regulation of coronary blood flow. *Compr Physiol.* 2017;7:321-382.
9. Halcox JP, Schenke WH, Zalos G, Mincemoyer R, Prasad A, Waclawiw MA, Nour KR, Quyyumi AA. Prognostic value of coronary vascular endothelial dysfunction. *Circulation.* 2002;106:653-658.
10. van Wolferen SA, Marcus JT, Westerhof N, Spreeuwenberg MD, Marques KM, Bronzwaer JG, Henkens IR, Gan CT, Boonstra A, Postmus PE, Vonk-Noordegraaf A. Right coronary artery flow impairment in patients with pulmonary hypertension. *Eur Heart J.* 2008;29:120-127.
11. Kim HJ, Yoo HY. Hypoxic pulmonary vasoconstriction and vascular contractility in monocrotaline-induced pulmonary arterial hypertensive rats. *Korean J Physiol Pharmacol.* 2016;20:641-647.
12. Farber HW, Loscalzo J. Pulmonary arterial hypertension. *N Engl J Med.* 2004;351:1655-1665.
13. Stenmark KR, Meyrick B, Galie N, Mooi WJ, McMurtry IF. Animal models of pulmonary arterial hypertension: the hope for etiological discovery and pharmacological cure. *Am J Physiol Lung Cell Mol Physiol.* 2009;297:L1013-L1032.
14. Rabinovitch M. Monocrotaline-induced pulmonary hypertension in rats. In: Simon DI, Rogers C, editors. *Vascular disease and injury*: *preclinical research*. *Totowa*: *Humana Press*; 2001. p. 261-280.
15. Boucherat O, Chabot S, Antigny F, Perros F, Provencher S, Bonnet S. Potassium channels in pulmonary arterial hypertension. *Eur Respir J.* 2015;46:1167-1177.
16. Nakazawa H, Hori M, Ozaki H, Karaki H. Mechanisms underlying the impairment of endothelium-dependent relaxation in the pulmonary artery of monocrotaline-induced pulmonary hypertensive rats. *Br J Pharmacol*. 1999;128:1098-1104.
17. Xie L, Lin P, Xie H, Xu C. Effects of atorvastatin and losartan on monocrotaline-induced pulmonary artery remodeling in rats. *Clin Exp Hypertens.* 2010;32:547-554.
18. Meloche J, Lampron MC, Nadeau V, Maltais M, Potus F, Lambert C, Tremblay E, Vitry G, Breuils-Bonnet S, Boucherat O, Charbonneau E, Provencher S, Paulin R, Bonnet S. Implication of inflammation and epigenetic readers in coronary artery remodeling in patients with pulmonary arterial hypertension. *Arterioscler Thromb Vasc Biol.* 2017;37:1513-1523.
19. Gautier M, Hyvelin JM, de Crescenzo V, Eder V, Bonnet P. Heterogeneous Kv1 function and expression in coronary myocytes from right and left ventricles in rats. *Am J Physiol Heart Circ Physiol*. 2007;292:H475-H482.
20. Morales-Cano D, Moreno L, Barreira B, Pandolfi R, Chamorro V, Jimenez R, Villamor E, Duarte J, Perez-Vizcaino F, Cogolludo A. Kv7 channels critically determine coronary artery reactivity: left-right differences and down-regulation by hyperglycaemia. *Cardiovasc Res.* 2015;106:98-108.
21. Hyvelin JM, Gautier M, Lemaire MC, Bonnet P, Eder V. Adaptative modifications of right coronary myocytes voltage-gated K^+ currents in rat with hypoxic pulmonary hypertension. *Pflugers Arch.* 2009;457:721-730.
22. Lee S, Yang Y, Tanner MA, Li M, Hill MA. Heterogeneity in Kv7 channel function in the cerebral and coronary circulation. *Microcirculation.* 2015;22:109-121.
23. Quayle JM, Dart C, Standen NB. The properties and distribution of inward rectifier potassium currents in pig coronary arterial smooth muscle. *J Physiol.* 1996;494 (Pt 3):715-726.
24. Park WS, Han J, Kim N, Ko JH, Kim SJ, Earm YE. Activation of inward rectifier K^+ channels by hypoxia in rabbit coronary arterial smooth muscle cells. *Am J Physiol Heart Circ Physiol.* 2005;289:H2461-H2467.
25. Smith PD, Brett SE, Luykenaar KD, Sandow SL, Marrelli SP, Vigmond EJ, Welsh DG. KIR channels function as electrical amplifiers in rat vascular smooth muscle. *J Physiol.* 2008;586:1147-1160.